https://doi.org/10.1016/j.seppur.2017.08.060

Transition from depth to surface filtration for a low-skin effect filter subject to continuous loading of nano-aerosols

Wallace Woon-Fong Leung*, Hung-Faat Choy

The Hong Kong Polytechnic University

Hung Hom, Hong Kong

*Corresponding author, Email: mmwleung@polyu.edu.hk

Keywords: depth-to-surface filtration transition; low-skin effect; nanofiber filter; nano-aerosols; aerosol bridging

Abstract

A thin, highly porous, nanofiber filter with low-pressure drop start out in “depth filtration” in a clean state with aerosols mostly captured by the fibers in the filter. For nanofibers with high capture efficiency, the fibers in the region upstream of the filter facing the challenging aerosol flow tends to capture more aerosols. The capture aerosols in turn can capture more incoming aerosols in this region leaving much less aerosols escaping downstream of the filter. Furthermore, these captured aerosols, forming dendritic structures, reduce the size of flowable pores in the region. This “skin region” upstream of the filter can be quite thin as compared to the entire filter thickness, yet it accounts for the large fraction of the aerosols captured in the filter as well as large fraction of the pressure drop across the filter. With more aerosols loading, the openings of the flowable pores in the skin region get blocked by aerosol dendrites that bridge across captured aerosols and fibers. These aerosol bridges subsequently build-up above the filter surface in the “surface filtration” regime. As more aerosol bridges stack-up on existing ones and interact with each other, they form ultimately a continuous cake layer on the filter surface.

The pressure drop due to the skin effect, which is a combination of both pore filling in the skin region in the filter and the aerosol bridges, can be relatively low (i.e. low-skin effect) for low nanofiber packing density and a thin nanofiber filter. However, the establishment of the skin region during depth filtration and the aerosol bridging effect above the filter surface are still two essential processes prior to formation of the cake on the filter surface. Two experiments and related analysis on loading of thin nanofiber filters using nano-aerosols are used to investigate this scenario. It has been found that in the course of aerosol bridging, the pressure drop behaves predominantly concave upward with increasing specific aerosol deposit. This contrast with previous study with high-skin effect for a thick, less-porous nanofiber filter for which aerosol bridging predominantly yields a concave downward behavior with specific aerosol deposit during pressure drop excursion. Most importantly, the bridging model that predicts successfully the high-skin effect can also predict the low-skin effect where pressure drop has a concave upward behavior with increasing specific aerosol deposit. Finally, we have demonstrated the aerosol holding capacity for a thin, highly porous, nanofiber filter can still be significant, with a small fraction of the total aerosols captured by depth filtration in the filter, and majority of deposited aerosols above the filter in the surface filtration regime, partly in the aerosol bridges and mostly in the cake.

1. Introduction

Airborne viruses (from common influenza, bird flu, swine flu, SARS to MERS etc.), small bacteria (tuberculosis), pollutant particulates from combustion (power plants, vehicles etc.) are of size approximately 100 nanometers (which is 1000 times smaller than human hair). These "nano-aerosols" can be inhaled readily by human leading to chronic respiratory and cardiovascular diseases [1-3]. Some of these pollutant particles are also formed from chemical reaction of harmful pollutant gases, such as nitrogen oxide, hydrocarbon and volatile organic compounds. In the presence of sunlight, they form irritating smog particles of sizes 100 to 1,000 nanometers that cause visibility impairment. Over 45 cities

in Mainland China and numerous cities in Asia are faced with serious smog problems that affect literally millions of inhabitants, especially elderly with respiratory diseases, let alone the impact on the economics.

Filters made of nanofibers are excellent for capturing of these nano-aerosols especially the enhanced surface area can enhance interception and diffusion capture [4]. When a nanofiber filter has to be deployed for long-term loading such as for airplanes, vehicles, trains or in offices, auditoriums, living spaces, and wards, the filter has to start out capturing challenging aerosols in the filter in a depth-filtration mode. At some point, the filtration mode changes from depth to surface filtration where the filter cake that forms on the filter surface becomes the effective filtration media. In general, we can divide this process into three stages - a depth filtration mode, a transition mode and a surface filtration mode. In early studies of nanofiber filter, it has been established that even in the depth filter mode not the entire filter is uniformly loaded with aerosols. More aerosols get captured in a thin “skin region” upfront of the filter facing the incoming aerosol flow. These trapped aerosols in turn become the sites for capturing more aerosols. This leads to an avalanche effect that more aerosols get trapped in the skin layer rapidly building up high pressure drop across the layer [5]. This pressure drop can account for 80-90% of the pressure drop of the entire filter similar to the case of liquid filtration. A study has been made to investigate transition from depth to surface filtration using a high efficiency nanofiber filter that has grade efficiency of over 50% for 300nm aerosol [6]. It is assumed that the transition primarily takes place in the skin for which the flowable pores in the skin region get aerosol deposit reaching a level for which further incoming aerosols would bridge over the flowable pores or capillaries. This is the starting point of the transition. As more aerosols challenge the filter, more aerosol bridges are built and they start to stack-up above the filter. Neighboring stack-up aerosol bridges interact with each other eventually forming a continuous cake layer across the filter surface. At this point, further incoming aerosols get trapped completely by the cake layer. This is the end of transition and beginning of cake

filtration. Hereafter, the pressure drop across the cake layer is dictated by the aerosols packing arrangement in the cake and the cake thickness. A schematic showing the filling of the capillaries in the skin layer of the filter [7], bridging [6], and cake formation is shown in Fig. 1a. Needless to say, the latter is an over-simplification of what is happening but does reveal the complicated transition between depth and surface filtration. As shown in Fig. 1a, the aerosol bridges in the transition region start to spread out laterally and they interact to form eventually a continuous cake layer. By several case study examples in an early study [6], it has been shown that the pressure drop excursion curve in the transition results in a concave downward behavior, which is illustrated in the top part (dash curve) of the pressure drop excursion curve plotted against specific aerosol loading in Fig. 1b. This scenario has been referred as the "high-skin effect", i.e. high Δp_s in Fig. 1b, for a nanofiber filter with high-fiber packing, thicker filter, and high initial pressure drop.

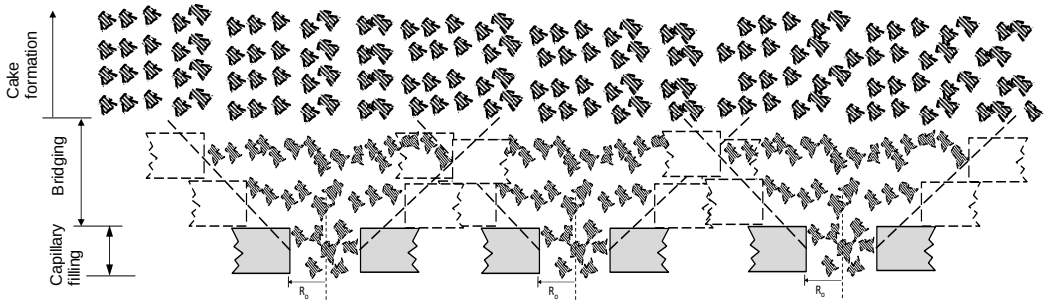

Fig. 1a – Schematic of capillary filling, bridging, and cake formation.

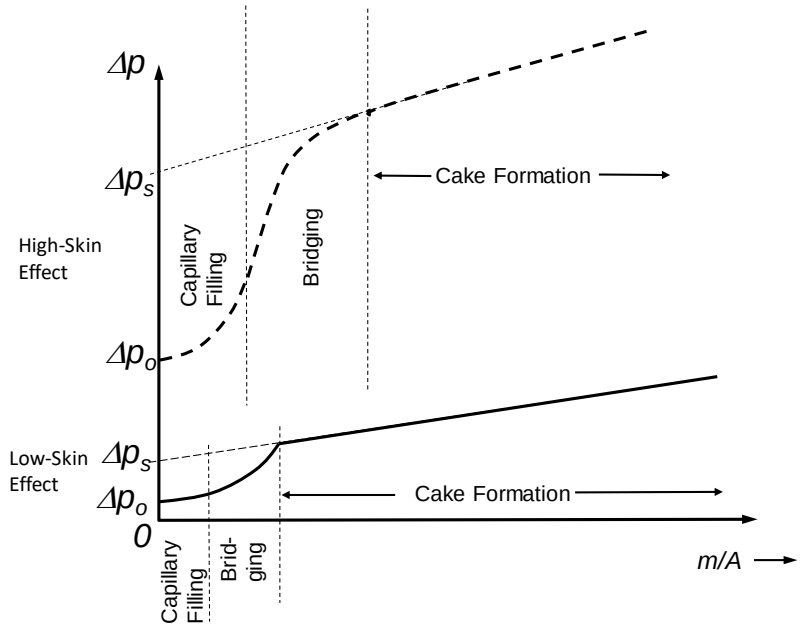

Fig. 1b – Pressure excursion behavior during aerosol loading of a nanofiber filter including capillary filling in the skin layer, bridging across the capillaries/pores extending beyond the filter surface, and full cake layer formation across the filter surface. The pressure excursion for both low-skin and high-skin effect cases are illustrated.

Several interesting issues begin to surface, which are listed below:

1. When the skin effect is low, such as a nanofiber with initial low efficiency, say less than 20%, would there be a transition from depth to surface filtration provided sufficiently long aerosol loading?
2. If (1) holds, what would be the behavior of the pressure excursion curve? Would it the same as the dash curve with concave downward behavior in the bridging regime similar to the high-skin effect case, i.e. large Δp_s? Or would it be completely different?
3. If (1) holds, is there a skin region that plays an important role in the transition from depth to surface filtration?

4. If (1) holds, would the previous capillary and bridging models still describe the correct pressure drop excursion behavior?

Indeed, we will address these interesting issues by showing that under low-skin effect with a nanofiber filter that starts out with efficiency (for 300nm NaCl) of less than 20%, with sufficient nano-aerosol loading, the filter can still change from depth to surface filtration. The pressure drop excursion curve versus specific aerosol loading may not conform to the previous study for the high-skin (large Δp_s), where the pressure drop first increases rapidly, subsequently changing to a concave downward behavior which ultimately leads to a linear trend exhibiting cake filtration, see dash curve on upper of Fig. 1b. Instead, the pressure drop rises from an initial low Δp_o corresponding to the pressure drop of a clean filter media; it continues to rise in a concave upward behavior in both the capillary filling and bridging regimes, and ultimately leads to a linear pressure drop trend when the cake layer starts to form. This is illustrated by the solid curve in the bottom part of Fig. 1b with a smaller extrapolated Δp_s. This low-skin effect case is quite a contrast when compared to the dash curve for the high-skin case with large Δp_s. We will also show that the skin layer also plays a catalyst role in the capillary filling and transition from depth to surface filtration, same as with the high-skin Δp_s case. The capillary model [7] can still describe the initial pressure buildup during filling of the capillary pores. The bridging model can still correctly describe the aerosol bridging behavior and the geometric factor *g* takes on either a small positive value and at times even negative value, giving rise to a concave upward pressure drop curve. Both experiments and modelling are used to complement each other in the study. Two low-skin nanofiber filter cases will be used in the present study, one corresponding to an initial nominal pressure drop of 15Pa and the other only 7Pa both under face velocity of 0.053ms^{-1}. These are much lower than the initial pressure drop of 28-35Pa clean filters with the high-skin effect [6].

2. Experimental Setup

2.1 Nano-aerosol generation

A submicron aerosol generator is used to generate sodium chloride aerosols 50 to 400nm with concentration no lower than 10,000 #/cm^3. The aerosols were dried in a membrane dehumidifier before loading the filter. The filter mounted in a test column has a diameter of 7 cm. The loading was interrupted periodically and aerosols were generated for grade efficiency testing. The test aerosols were produced by classifying aerosols below and above the test aerosol size using first an ionizer that impart charges to the aerosols, then classify the aerosol by charge/size in a Differential Mobility Analyzer (DMA) and subsequently neutralizing the outstanding charges by passing the aerosol stream again through a second ionizer. This concentrated aerosol stream with the test size was mixed with diluted air (after being filtered out of particles from a HEPA filter) before challenging the test filter. The concentration of particles was measured iso-kinetically, respectively, upstream and downstream of the filter using a condensation particle counter (CPC) from which the grade efficiency of the test aerosol was determined. The pressure drop across the filter was monitored by the digital pressure gages with continuous read-out sent to the computer. The setup of the aerosol generator and tester is shown in Fig. 2.

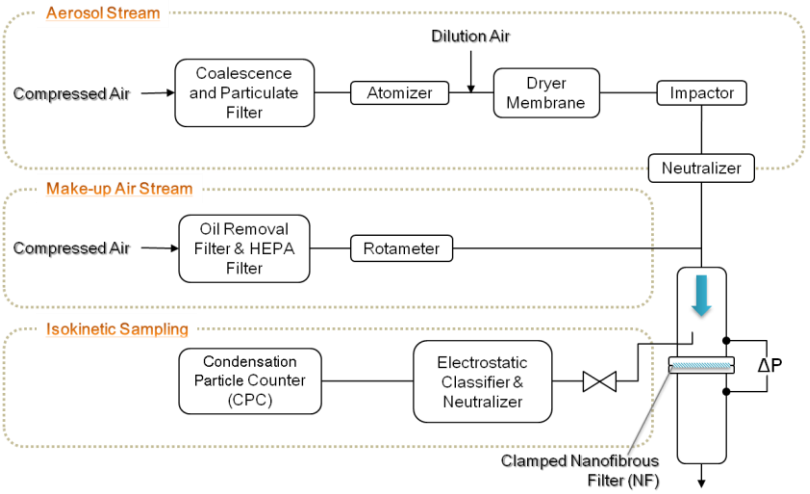

Fig. 2 – Submicron aerosol generator (SMAG) and filter tester for respectively, loading the test filter and making measurement on the grade efficiency of the filter.

2.2 Nanofiber filter production

Nanofiber filter were produced in-house by needle-less electrospinning process of Nylon 6, see Fig. A1 in Appendix A. The pellets of Nylon 6 were dissolved in formic acid. Different weight percent of Nylon 6 were used to produce nanofibers free from droplets with fiber diameter of 150 to 290 nm. High resolution scanning electron microscope (SEM) was used to take images of the electrospun nanofiber samples. For representative samples, 100 fibers were randomly selected and their diameter was statistically measured to produce the mean and standard deviation values.

2.3 Loading of a test filter

A thin, highly permeable, nanofiber filter was loaded with nano-aerosols with particle size in the range of 50-400nm. The mode of filtration started out with depth filtration and subsequently changed over to surface filtration. The pressure drop across the filter was closely monitored over loading. Also, periodically the grade efficiencies of the NaCl aerosols were tested to determine for a given size the amount of challenging aerosols being captured. In particular, the 300-nm aerosol was used as an indicator. Once the grade efficiency of the 300nm aerosol reached 99%, the filter was considered to change from depth to cake filtration for interpretation of the test. The loading will continue until the pressure drop reaches the maximum set between 800 and 900Pa. Two different sets of experiments were carried out on respectively, two clean nanofiber filters.

3 Modelling

3.1 Skin layer

Skin layer, a thin region upstream of the fiber matt, tends to be exposed first to the incoming aerosols. The captured aerosols become effective sites together with the original fibers in the skin region to

further trap more aerosols. This domino effect continues and most aerosols are trapped in the skin region and this region also accounts for majority of the pressure drop across the entire filter. The skin layer phenomenon is present in the filter no matter whether the nanofiber filter has a smaller diameter nanofiber or a sufficiently thin filter thickness.

3.2 Capillary filling model

A capillary filling model has been developed [7] to model the flowable pores in the skin layer. The interconnected flowable pores in the skin layer are modelled as a large number, *n*, of capillaries with average radius R_o. These capillaries are assumed to transverse across the entire skin layer with thickness *h*.

The aerosol deposit is assumed to be equivalent to the case when the aerosols are packed tight against the inner wall of the capillary uniformly and circumferentially, thereby reducing the effective radius *R* of the capillary from its initial radius R_o. The trapped aerosols filled the flowable pores to a point in which new aerosols start bridging across an already "neck-down" capillary. This initial bridging is assumed to take place when the pore cross sectional area is reduced to 60% of its original area. In other words, the capillary is 40% filled. The appropriate equations have been derived elsewhere [7] and is summarized below:

$$\frac{\Delta p}{\Delta p_o} = \frac{1}{(1-\xi)^2}; \qquad \xi \le 0.4$$

$$\Delta p_o = \frac{8\mu u h}{\phi_o R_o^{\,2}} \qquad \text{(1a-c)}$$

$$\xi = \frac{(m/A)}{\phi_o h \rho_s \varepsilon_s}$$

$$R/R_o = \sqrt{1-\xi}$$

$$n = \phi_o \left(\frac{R_f}{R_o}\right)^2 \qquad \text{(2a, b)}$$

3.3 Bridging model

Once aerosols start to bridge across the capillary opening, more aerosols will deposit on the initial aerosol bridge. Given these aerosol bridges are located above the filter surface, there is no lateral confinement. In the bridging model [7], the lateral extent is assumed to be $R_o' = R_o\left[1 + g(\xi - \xi_i)\right]$ where ξ is the filling parameter corresponding to the specific loading *m/A* by Eq. 1c, ξ_i is the incipient of bridging taken as 0.4, and *g* is the geometric factor governing the lateral extent of the aerosol bridges. When *g*=0, $R_o'=R_o$ and the lateral extent is the same as the original capillary and there is no widening of the aerosol bridge above the filter surface. When g>0, $R_o'>R_o$ this will give a concave downward behavior of the pressure drop excursion (dash line) curve as shown in the upper part of Fig. 1b. On the other hand, when *g*<0, $R_o'<R_o$ this will give a concave upward behavior of the pressure drop excursion (solid line) curve as shown in lower part of Fig. 1b. Thus, the total pressure drop is simply a sum of all the stack-up aerosol bridges as given by the second term in Eq. 3 starting from the incipient point of bridging. The first term is simply the pressure drop in the flowable pore in the skin layer at the incipient point of bridging from Eq. 1a. Thus the pressure drop in bridging is given by [6],

$$\frac{\Delta p}{\Delta p_o} = \frac{1}{\left(1-\xi_i\right)^2} + \sum_{j=1}^{n} \frac{1}{[1+g(\xi_{j+1}-\xi_i)]^2} \frac{1}{[1-\left(\xi_{j+1}-\xi_j\right)]^2} \qquad (3)$$

g in Eq. 3 is derived from matching the pressure prediction using Eq. 3 with the test data.

4. Results and Discussions

Two cases have been investigated in details to illustrate a low-skin effect nanofiber filter that evolves from depth to surface filtration. The capillary model and the bridging model are used to interpret the test data.

4.1 Case A

The polydispersed particle size distribution (PSD) between 50 and 500nm is a log-normal distribution as shown in Fig. 3 with the count mean diameter (CMD) being 128nm. The filter has a mean fiber diameter of 291nm and the initial pressure drop Δp_o is only 15.8Pa.

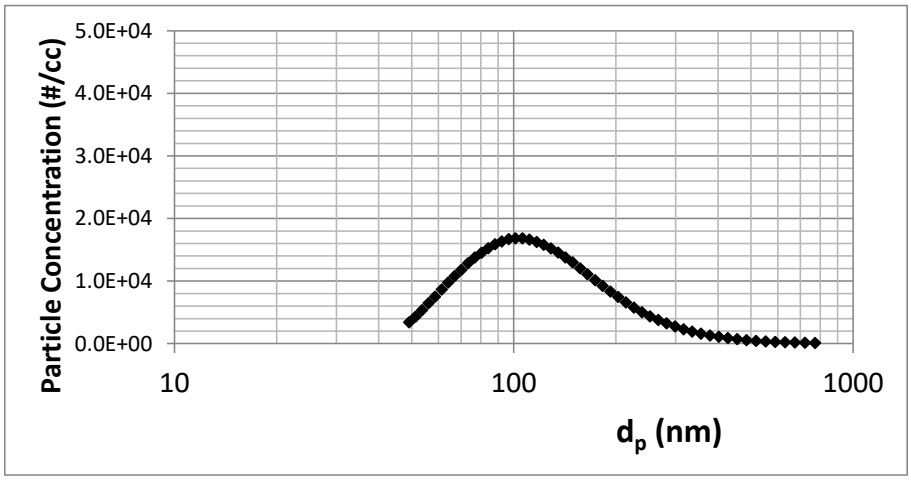

Fig. 3 – Particle size distribution of challenging NaCl aerosols challenging the nanofiber filter

When matching the test data with the capillary model, i.e. modelling the flowable pores with aerosol deposit, we need to dimensionalize all the test pressure measurement by dividing with Δp_o from ξ=0 to $\xi\approx$0.4. The best match between capillary model prediction and the normalized test data yields the skin layer thickness h=2.2μm as shown in Fig. 4. It is evident in Fig. 4 that the test data start to fall below the capillary model prediction, that has much higher pressure drop beyond ξ=0.4. As ξ>0.4, the capillary is so filled with captured aerosols that incoming aerosols start to bridge over the opening of the capillary. This will be predicted by the bridging model to follow.

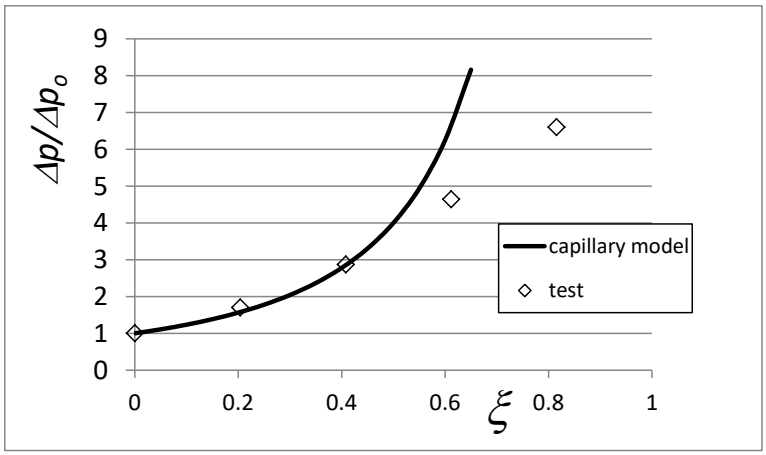

Fig. 4 – Matching capillary model with the pressure drop test data.

One interesting result from the capillary model is that from Eq. 1b,

$$R_o = \sqrt{\frac{8\mu u h}{\phi_o \Delta p_o}} \tag{4}$$

Given μ=1.81(10^{-5})kg(ms)$^{-1}$, u=0.053ms^{-1}, h=2.2μm (from matching), ϕ_o=0.97, Δp_o=15.8Pa, this gives R_o=1.05 μm, or the capillary diameter, which is $2R_o$, is 2.1 μm. Fig. 5 shows the scanning electron microscope (SEM) image of the test filter. As can be seen in Fig. 5, the average pore size is indeed approximately 2 μm. This is very encouraging.

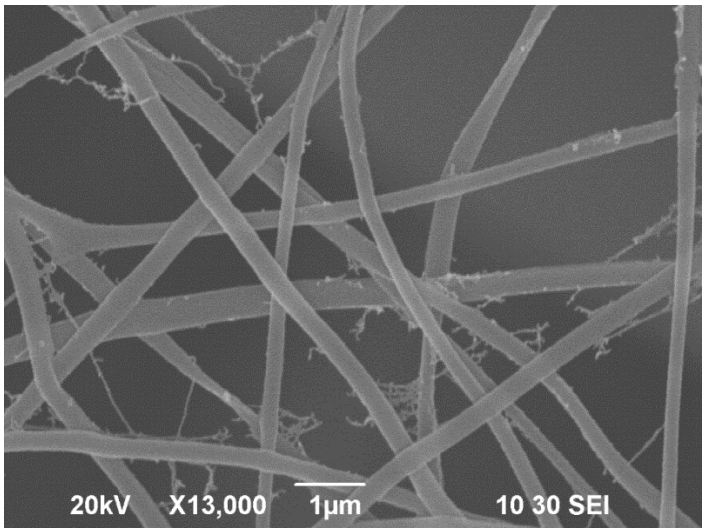

Fig. 5 – SEM image of the test sample for Case A. Average pore size is approximately 2 μm.

Beyond ξ=0.4, the bridging model is used to match the test data. First, we have to establish the cake filtration operating line. The cake equation is assumed to be valid when the grade efficiency of the representative aerosol 300nm reaches 100% which infers that all incoming 300nm aerosol are captured by the cake layer that acts as an active filter media. By then the original filter which has loaded aerosols serves only as a mechanical support. By matching with the data for the cake after the 300nm aerosol has reached 100%, the cake equation is determined to be

$$\Delta p = 55 + 38(m/A) \qquad (5)$$

where *m/A* is expressed as gm^{-2} and Δp in Pa. Next, we need to match the bridging model prediction to the test data in the bridging regime and this also serves as a continuity of the capillary model prediction. Most importantly, the bridging model prediction has to provide a smooth continuity with the linear cake equation. We have been able to tune the adjustable geometric parameter *g* to achieve these two goals. Figs. 6a and 6b show the mismatch of model prediction with experiments at *g*=0 and *g*=0.2, respectively. When *g*=0, the bridging model over-predicts the pressure drop test data, and also the bridging model prediction cannot provide a continuous smooth transition to the cake filtration "line", see Fig. 6a. When *g*=0.2, the bridging model under-predicts the pressure drop test data, and the bridging model prediction again cannot provide a continuous smooth transition to the cake filtration line. In both cases, there is a discontinuity in value and slope between the bridging and cake filtration prediction, Eq. 5, which is undesirable. When *g*=0.1 as shown in Fig. 6c, there is good match of the test data in the bridging regime as well as good continuity in value and slope between the bridging and cake filtration prediction. There is no "kink" (discontinuity in slope) at the common junction of the two predictions! In Fig. 6c, it can be seen that there is a slight concave downward behavior as predicted by the bridging model. In between the capillary model, that predicts a concave upward behavior, and bridging model, that predicts a slight

concave downward behavior, is a weak inflection point. This is much less distinct compared to the case of deploying a high-efficiency nanofiber filter [6]. Another very interesting aspect is that a nanofiber filter that starts out at low efficiency, of 16.8% based on 300nm challenging aerosols, can be loaded with polydispersed nanoaerosols to a point at which it transits from depth to surface filtration. In the due course of aerosol loading, initially the aerosols deposit in the flowable pores in the skin region of the filter up to a certain level. Further deposition of aerosols results in bridging across the pore openings or capillaries. Additional challenging aerosols will only deposit on these bridges resulting in a continuous layer of aerosol cake forming on the filter surface. This process is identical to that of loading the "high-skin" nanofiber filter [6], except there is no strong concave behavior in the pressure drop especially in the "bridging" regime.

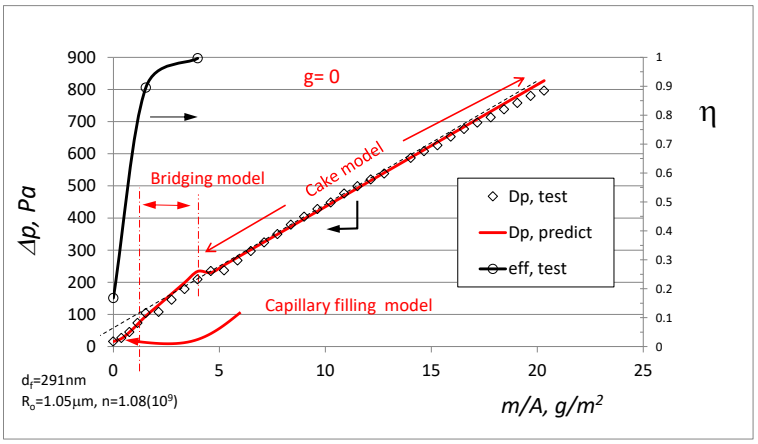

Fig. 6a – *g*=0 which gives incorrect match as it cannot catchup with the cake slope.

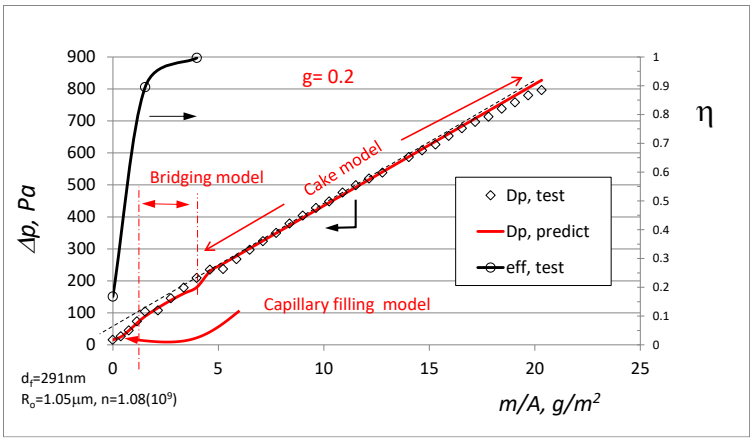

Fig. 6b – g=0.2 which underpredicts the performance and also do not provide smooth transition to cake filtration.

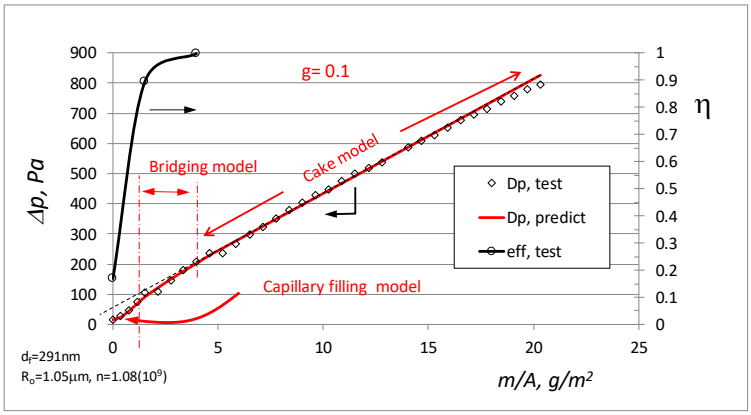

Fig. 6c – The parameter g=0.1 provides a good match with test data and provides a smooth transition to the cake filtration line

A closer look at the dimensionless pressure $\Delta p/\Delta p_o$ versus ξ in the capillary filling and bridging regimes is shown in Fig. 7. The capillary model is valid up to 0.4 for which we assume the bridging of aerosols starts and the bridging model takes over in predicting the bridging behavior. The bridging model is valid until the measured efficiency (300nm aerosol) reaches 100%, which for this case corresponds to ξ=2.15. The slightly concave downward behavior of the dimensionless pressure drop curve is evident in Fig. 7.

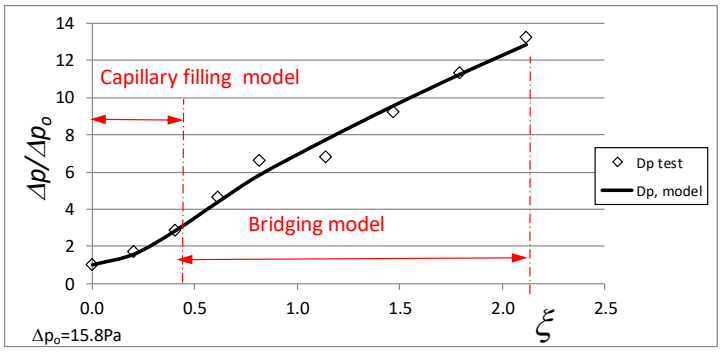

Fig. 7 – After matching with g=0.1, this figure displays the comparison with the data and the slight concave downward behavior on the pressure drop in the bridging process.

The cake thickness can be determined from Appendix B. The calculated cake thickness based on the experimental pressure drop as a function of specific loading is shown by the bottom curve in Fig. 8. This is an inferred value assuming the properties of the cake remain unchanged and that the Ergun equation is valid for the pressure drop across the porous media. As can be seen, despite the pressure drop varies linearly with specific mass, the thickness of the cake due to the non-linearity of the pressure drop equation does not vary linearly with the specific mass deposit. Given this is less than a millimeter, it would be difficult to make such measurement in-situ during the experiment, and especially for a fragile and delicate thin cake.

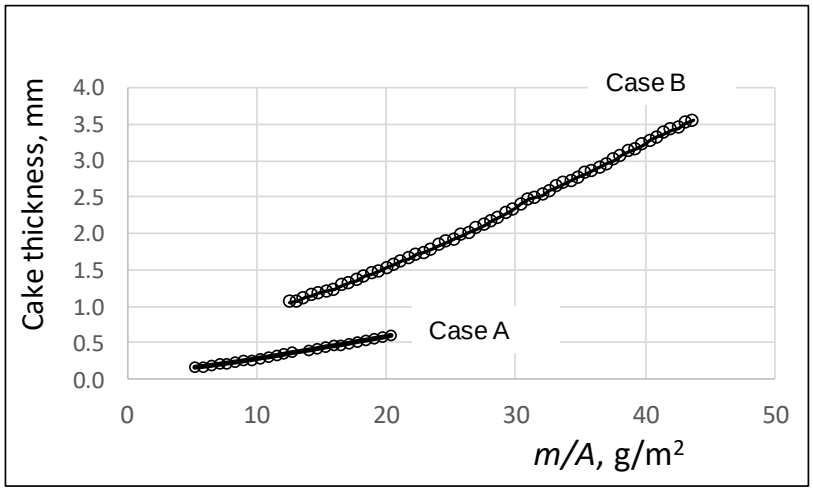

Fig. 8 – Cake thickness as a function of specific mass deposition on the nanofiber filter.

4.2 Case B

In this case, we are interested to see when an even thinner nanofiber filter is used can it ever reach transition from depth to surface filtration for which a cake forms on the filter surface?

The filter selected has a sparse nanofiber network as shown by the SEM image in Fig. 9a and 9b. There are only several layers of nanofibers. The clean nanofiber pressure drop is rather low, only 7.2Pa despite the average fiber diameter is 150nm. The pore diameter is large and thus the media is quite permeable with low pressure drop across the filter.

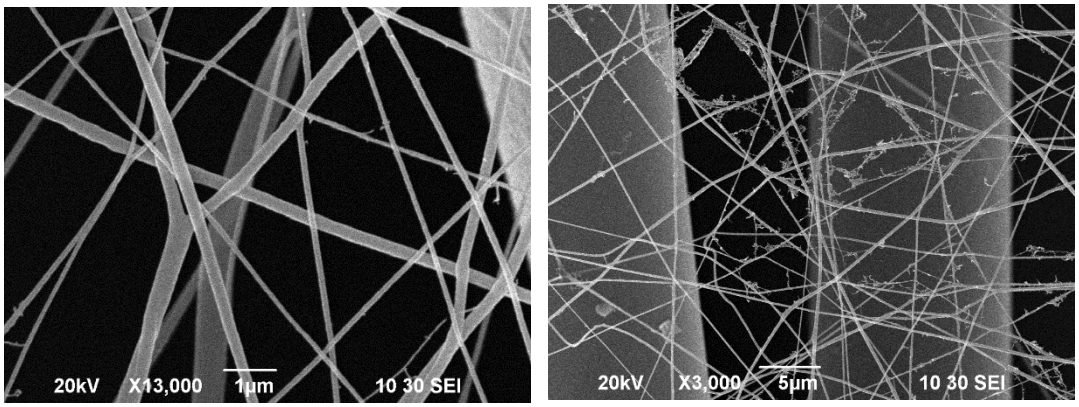

Fig. 9 (a) zoom-in image of nanofiber filter showing pore size of 3 micrometers. (b) zoom-out image showing a larger area where pore size is under 5 micrometers.

The test aerosol has CMD of 124nm and the size distribution is not too far off from that shown in Fig. 1. The skin layer thickness h can be determined by matching the capillary model to the test data. The thickness h turns out to be 3μm after matching the capillary model with the test data in Fig. 10.

Given μ=1.81(10^{-5})kg(ms)$^{-1}$, u=0.053ms^{-1}, h=3μm (from matching), ϕ_o=0.97, Δp_o=7.2Pa, this gives R_o=1.85 μm. Therefore, the capillary diameter, which is $2R_o$, is 3.6 μm. Figs. 9a, b shows the scanning electron microscope (SEM) image of the filter under test. As can be seen in these figures, the average

pore size is indeed approximately 3 to 5 μm bracketing the model prediction of the pore size of 3.6 μm. The reason why the pore size is larger in Case B is that there are only several layers of nanofibers and this is also the same reason for the low pressure drop albeit the fiber diameter is smaller, 150nm.

Despite this, the interesting aspect is to see if indeed transition from depth to cake filtration can take place during continuous loading. Fig. 11a-c show the test data which reveals that at m/A =12 gm^{-2}, the efficiency for the 300nm aerosol has already reached 100%. Thereafter, the filter is operated under cake filtration up to the end of loading with m/A=43 gm^{-2}.

We have been able to tune the adjustable geometric parameter g to achieve matching of the bridging model prediction with the test data. Also, the prediction in bridging provides a smooth transition to cake filtration. It may be useful to show two negative cases to demonstrate the sensitivity on matching the model to the experimental measurements. First, Figs. 11a and 11b show the mismatch of model with experiments (both with negative g) at g=-0.1 and g=-0.02, respectively. When g=-0.1, the bridging model over-predicts the pressure drop test data, and also the bridging model cannot provide a continuous smooth transition to the cake filtration line. On the other hand when g= -0.02, the bridging model under-predicts the pressure drop test data, and further the bridging model cannot provide a continuous smooth transition to the cake filtration line. In both cases, there is a discontinuity in value and slope between the bridging and cake filtration prediction, which is undesirable. Finally, in Fig. 11c when g= -0.05, there is good matching of the test data as well as a good continuity in value and slope between the bridging and cake filtration prediction. Interestingly, in Fig. 11c, the bridging model prediction provides a concave upward behavior matching that of the test data. This is rather remarkable! Note here that the g value is slightly negative meaning the width of the bridges is actually slightly reducing as compared to those of the original capillaries in the skin layer of the filter. Further concave upward

behavior implies that each bridge layer has increasingly pressure drop due to the continuous narrowing down of its width. There are a total of 19 stack-up bridges in the bridging regime above the surface of the filter.

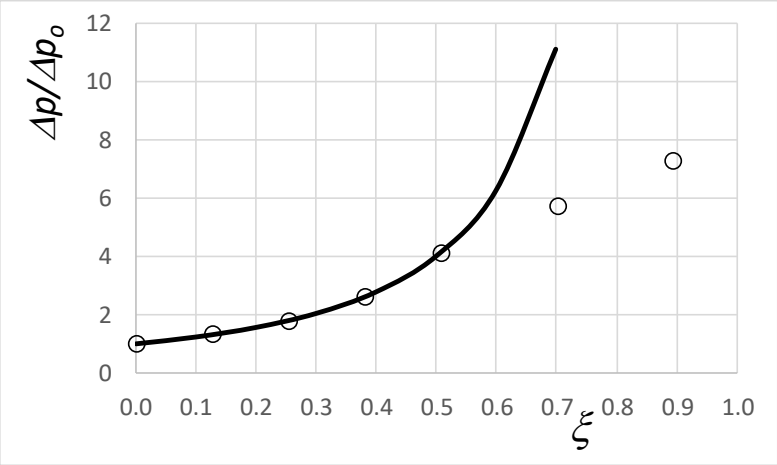

Fig. 10 – Matching capillary model with the test data.

Fig. 12 shows the details of the dimensionless pressure drop versus the filling parameter. The concave upward behavior of the data is reasonably well matched by the bridging model. It shows that there are as much as 19 stack-ups of the aerosol bridges involved in building ultimately a continuous cake layer above the filter surface.

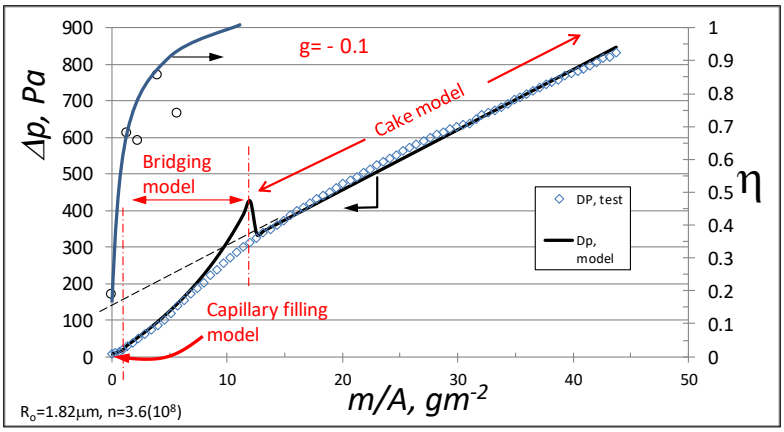

Fig. 11a – *g*= -0.1 over-estimates the actual pressure drop.

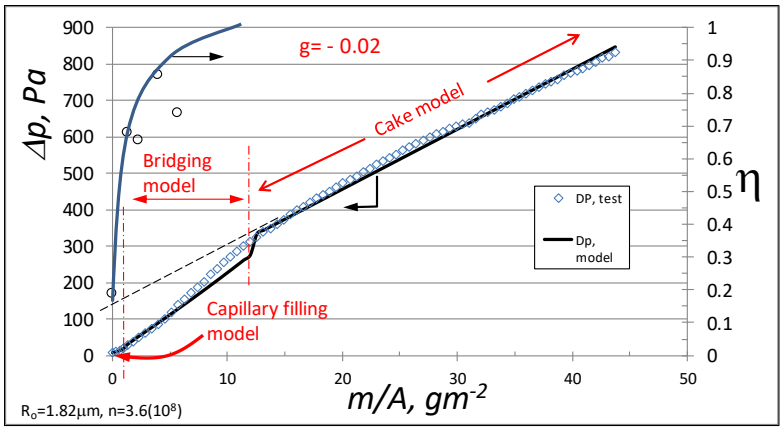

Fig. 11b – *g*= -0.01 under-estimates the actual pressure drop.

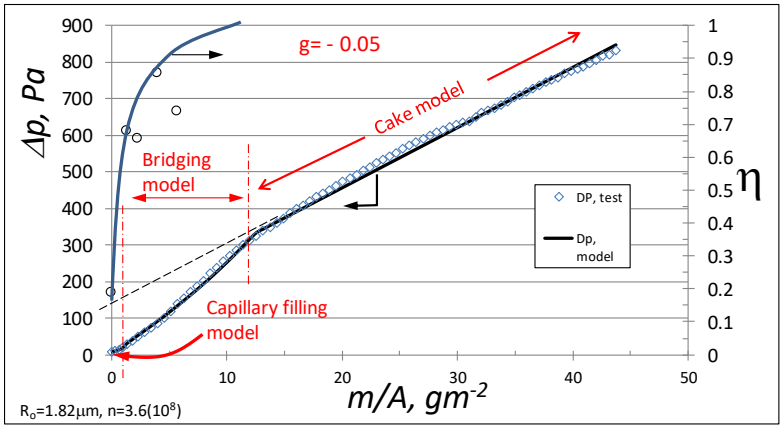

Fig. 11c – *g*= -0.05 matches with the actual pressure drop.

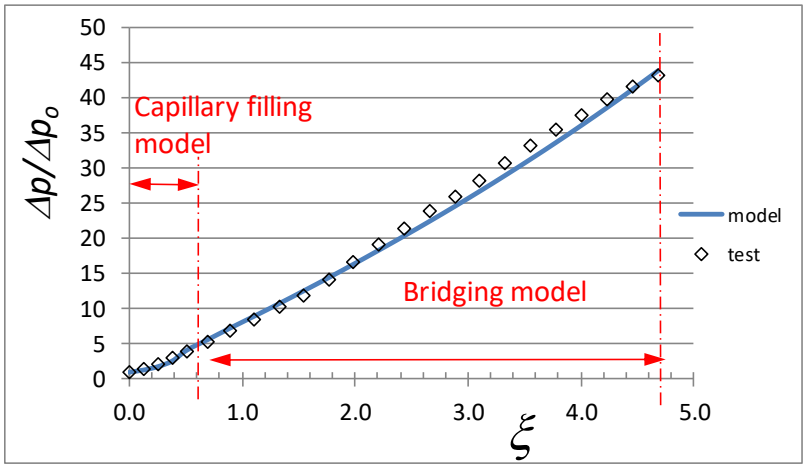

Fig. 12 – Details of the bridging model and capillary model predictions versus test data on pressure drop.

We have carried out similar calculations on cake thickness (Appendix B) and Fig. 8 (top curve) shows the cake can be as much as four millimeters thick on an otherwise thin nanofiber mat consisting of perhaps only 4-5 layers of nanofibers. The cake layer provides the aerosol storage capacity for the thin nanofiber filter.

Lastly, an interesting aspect is that the aerosols by mass captured in the nanofiber (serving as depth filter) amount to only 1.5 gm^{-2}, in the aerosol bridges 10.8 gm^{-2} and in the cake 31.4 gm^{-2}. Given the total *m/*A is 43.7 gm^{-2}, this reveals only 3% of aerosol by mass is filtered by the nanofiber (primary in the skin layer), 25% in the aerosol bridges (above the filter), and 72% in the cake (above the filter). It is quite remarkable that predominantly the trapped aerosols are outside the nanofiber filter. This means that the nanofiber mat does not need to be too thick to enhance aerosol holding capacity and it still can have high storage capacity of nano-aerosols, but mostly in surface filtration - some in the aerosol bridges and majority in the cake layer, both of which are above the filter.

5. Conclusions

We have demonstrated a low-skin nanofiber filter (highly porous, thin nanofiber mat) can start out with depth filtration and ultimately building up a full cake on the filter surface. The demonstration was carried out using two test cases both having a low initial pressure drop clean nanofiber filter with 7 to 15 Pa at challenging air velocity of 0.053ms^{-1}.

For one case with a thin nanofiber filter having initial pressure drop of 7Pa at 0.053ms^{-1} challenging air velocity, the cake can be several millimeters thick due to long-term loading of nano-aerosols. In other words, the nanofiber filter can have high loading capacity with captured aerosols stored in the cake and

not in the filter. In the transition between the capillary/pore filling and the cake formation, aerosol bridges form and they stack-up on top of each other. The lateral extent of these aerosol bridges are slightly reduced (geometric factor *g* negative) as they buildup above the filter surface giving rise to a concave upward behavior of the pressure drop. This concave upward behavior in the transition is well supported by the pressure drop measurements.

In another case, the fiber mat is thicker with a higher initial pressure drop for the clean filter with pressure drop of 15-16Pa, the bridging regime has a very slight concave downward behavior. Therefore, it can be concluded that for low-skin effect nanofiber filter, during the transition from initial pore filling to cake filtration, the pressure drop can be concave upward to slightly concave downward due to aerosols bridging. This is different when compared with a high-skin effect nanofiber filter with strong concave downward behavior in the transition/bridging regime.

The capillary and bridging model have demonstrated their applicability even in the low-skin effect (or low initial pressure drop) nanofiber filter. Instead of the perceived concave downward behavior associated with high-skin filter, the bridging regime can be slightly concave downward to even concave upward. This is quite interesting.

In any case, regardless of low- or high-skin effect nanofiber filter, the skin layer in the filter plays a critical role in the capillary filling in both cases, which ultimately leads to bridging on the filter surface with consequence of cake formation.

Also, the aerosol holding capacity even for a thin nanofiber filter with low-skin effect can be significant. The aerosols are primarily stored outside the filter, partly in the aerosol bridges, and mostly in the cake layer.

Acknowledgements

The authors want to thank the Hong Kong Research Grant Council in supporting the project under PolyU 518012.

Nomenclature

A filter area, [m^2]

h skin thickness, [m]

g geometric factor, [-]

k permeability, [m^2]

n number of capillaries, [-]

m mass, [kg]

p pressure, [Pa]

R capillary radius, [m]

s slope, [$Pa/(gm^{-2})$]

t time, [s]

u face velocity, [ms^{-1}]

Greek

α specific cake resistance [mkg^{-1}]

Δ change

ρ density, [kgm^{-3}]

ϕ porosity, [-]

ε solid volume fraction

η capture efficiency, [-]

ξ filling factor, [-]

μ viscosity, [$kg.m^{-1}s^{-1}$]

Subscript

c cake

f filter

i incipient to bridging

o before aerosol loading, m=0

s cake, solid, skin

References

[1] Mark R. Miller et al., "Inhaled nanoparticles accumulate at sites of vascular disease", ACS Nano, 11(5), pp 4542-4552, 2017.

[2] James C. Bonner, "Nanoparticles as a potential cause of pleural and interstitial lung disease", Proc. Am Thorac Soc., 7(2): 138-141, 2010.

[3] Marie-Claude Jaurand et al., "Mesothelioma: Do asbestos and carbon nanotubes pose the same health risk? Part Fibre Toxicol. 6:16, 2009.

[4] WWF Leung, CH Hung, and PT Yuan, "Effect of face velocity, nanofiber packing density and thickness on filtration performance of filters with nanofibers coated on a substrate" Separation and Purification Technology, 71, 30-37, 2010

[5] WWF Leung, CH Hung, "Skin effect in nanofiber filtration of submicron aerosols", Separation and Purification Technology, 92, 174-180, 2012.

[6] WWF Leung and HF Choy, "Transition from depth-to-surface filtration for a high-efficiency, high-skin, nanofiber filter under continuous nano-aerosol loading", submitted for publication.

[7] WWF Leung and CWY Hau, “Skin layer in cyclic loading-cleaning of a nanofiber filter in filtering nano-aerosols,” Separation and Purification Technology, 188, 367-378, 2017, doi: http://dx.doi.org/10.1016/j.seppur.2017.07.043

Appendix A

Test filters made of nanofibers with mean diameter of 150-290nm were used in the experiments. The filters were produced with needle-less electrospinning using a rotating electrode made up of 8 wires dipping successively into a precursor solution (nylon 6 pellets dissolved in formic acid) in a trough drawing out the liquid solution into a thin liquid film coating on the wires in the open air, see Fig. A1. When the electrical force from the set-up high-voltage field is greater than the capillary force acting on the thin liquid film, fibers start to form. The fibers will be drawn into progressively smaller diameter during free flight to the collecting electrode by virtue of combined electrostatic repulsion of charges left on the fiber and evaporation of the solvent. The typically consistency of nylon 6 solutions is 18-24% g/cm^3 with increasing concentration producing nanofibers with larger diameter. The rotation rate of the electrode was typically 10 to 15 hz, separation distance between the rotating electrode and the ground electrode with collection of nanofibers by a substrate mat was 15 to 19cm. The maximum voltage of the positive rotating electrode was at 70,000v. The collection plate was ground. By combination of voltage difference, the rotating speed of the feed electrode, distance between the positive electrode and the ground, nanofibers free from droplets were produced with relatively uniform diameter for our test filter.

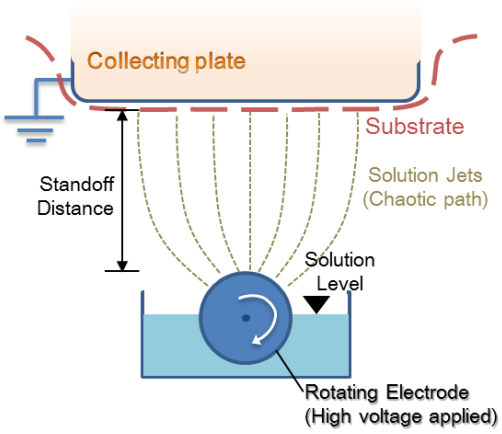

Fig. A1 - Schematic of needle-less electrospinning machine

Appendix B

Typical pressure drop excursion behavior is shown in Fig. B1.

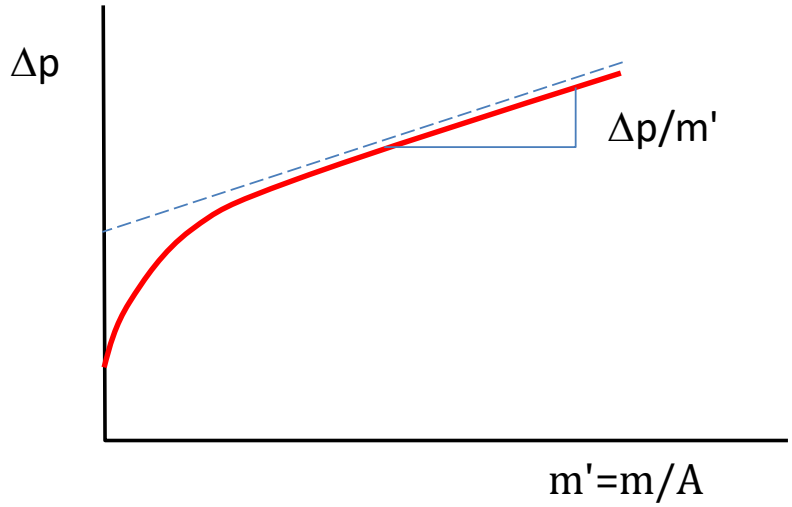

Fig. B1 – schematic of pressure drop focusing on cake behavior.

From the experimental plots for each case, we determine the slope at the linear segment corresponding to the cake deposited on the nanofiber filter, $\Delta p/m'$.

Take the Ergun equation, which is a simplified version of Carman-Kozeny equation,

$$\Delta p = \frac{150\mu}{d_p^2}\frac{{\varepsilon_s}^2}{(1-\varepsilon_s)^3}Lv \qquad \text{(B.1)}$$

where Δp is the pressure drop, L cake thickness, μ air viscosity, ε_s solidosity, v (=Q/A) the superficial velocity, d_p is the equivalent mass mean diameter of the cake particles (assumed spherical).

Material balance requires,

$$m = \rho_s \varepsilon_s AL$$
$$m' = m/A = \rho_s \varepsilon_s L \qquad \text{(B.2 and B.3)}$$

Eliminate L from the two equations, we get

$$\Delta p = \frac{150\mu}{d_p^2}\frac{\varepsilon_s{}^2}{(1-\varepsilon_s)^3}Lv = \frac{150\mu}{d_p^2}\frac{\varepsilon_s{}^2}{(1-\varepsilon_s)^3}\left[\frac{m'}{\rho_s\varepsilon_s}\right]v = \frac{150\mu}{d_p^2}\frac{\varepsilon_s}{(1-\varepsilon_s)^3}\left[\frac{m'}{\rho_s}\right]v$$

$$\left[\frac{\Delta p}{m'}\right]\frac{d_p^2}{150\mu}\frac{\rho_s}{v} = \frac{\varepsilon_s}{(1-\varepsilon_s)^3}$$

Rewriting,

$$1-(3+C)\varepsilon_s + 3\varepsilon_s{}^2 - \varepsilon_s{}^3 = 0, \quad \frac{1}{C} \equiv \left[\frac{\Delta p}{m'}\right]\frac{d_p^2}{150\mu}\frac{\rho_s}{v} \qquad \text{(B.4 \& B.5))}$$

The above can be solved numerically using Newton-Rapson method

Subsequently, L can be determined from

$$L = \frac{m'}{\rho_s \varepsilon_s} \qquad \text{(B.6)}$$

Thus, all the cake thickness and properties can be determined.